Inorganic Chemistry

Article

pubs.acs.org/IC

Single-Step Preparation of the Mixed Ba^{II}–Nb^{V} Oxides from a Heteropolynuclear Oxalate Complex

Marijana Jurić,* Jasminka Popović, Ana Šantić, Krešimir Molčanov, Nevenka Brničević, and Pavica Planinić*

Ruđer Bošković Institute, Bijenička cesta 54, 10000 Zagreb, Croatia

Supporting Information

ABSTRACT: A novel oxalate-based complex of the formula $\{Ba_2(H_2O)_5[NbO(C_2O_4)_3]HC_2O_4\}\cdot H_2O$ (**1**) was prepared from an aqueous solution containing the $[NbO(C_2O_4)_3]^{3-}$ and Ba^{2+} entities in the molar ratio 1:2, and characterized by X-ray single-crystal diffraction, IR spectroscopy, and thermal analysis. The crystal packing of **1** reveals a complex three-dimensional (3D) network: the Nb polyhedron is connected to eight neighboring Ba polyhedra through the oxalate ligands and the oxo-oxygen group, whereas the Ba polyhedra share edges and vertices. The ability of compound **1** to act as a single-source precursor for the formation of bimetallic oxides was investigated by the thermal analysis (TGA and DSC) and X-ray powder diffraction. Thermal processing of **1** resulted in the formation of mixed-metal oxide phases, $Ba_4Nb_2O_9$ and $Ba_5Nb_4O_{15}$. Three stable polymorphs of $Ba_4Nb_2O_9$ were isolated: the known, hexagonal α- and orthorhombic γ-$Ba_4Nb_2O_9$, and another one, not previously reported, hexagonal δ-$Ba_4Nb_2O_9$ polymorph. The new, δ-$Ba_4Nb_2O_9$ polymorph has the 6H-perovskite structure (space group $P6_3/m$), in which the $Nb_2O_9^{8-}$ face-sharing octahedral dimers are interconnected via corners to the regular BaO_6^{10-} octahedra. Formation of the mixed-metal oxides takes place at different temperatures: the $Ba_5Nb_4O_{15}$ oxide occurred at ~700 °C, as the major crystalline oxide phase; by heating the sample up to 1135 °C, the α-$Ba_4Nb_2O_9$ form was obtained, whereas the heating at 1175 °C caused the crystallization of two polymorphs, γ-$Ba_4Nb_2O_9$ and δ-$Ba_4Nb_2O_9$. Special focus was set on the electrical properties of the prepared mixed Ba^{II}–Nb^{V} oxides obtained by this molecular pathway in a single-step preparation.

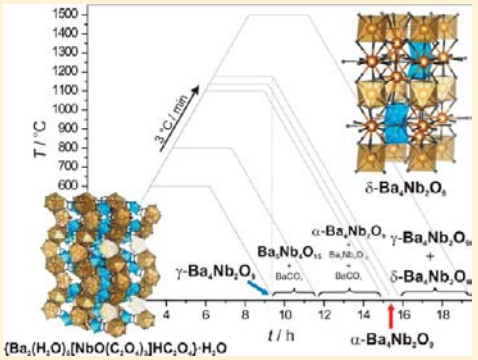

INTRODUCTION

In the design and synthesis of homo- and heteropolynuclear complexes as potentially new functional materials with desirable physical properties (mechanical, optical, electrical, or magnetic), an important role belongs to the oxalate $C_2O_4^{2-}$ anion because of its various possibilities of coordination to metal centers and the ability to mediate magnetic interactions between paramagnetic metal ions. So far, a huge number of oxalate-based transition metal species, of different nuclearity and dimensionality, have been synthesized and characterized.[1]

In the search for suitable synthetic routes leading to novel and promising polynuclear species, of considerable importance has been to find convenient mononuclear complexes that could be used as ligands toward other metal ions. Thus, the tris(oxalato)metalate anions, $[M^{III}(C_2O_4)_3]^{3-}$ (M^{III} = Cr, Mn, Fe, Ru, V), used as building blocks, represent a very efficient way for the synthesis of homo- and heterometallic oxalate-bridged two- (2D) and three-dimensional (3D) assemblies.[1] In our research group, for the first time, the tris(oxalato)-oxoniobate(V) anion, $[NbO(C_2O_4)_3]^{3-}$ was used for the same purpose providing a number of oxalate-based transition metal complexes.[2−4] The motive for selecting this anion as building unit was found in the capability of niobium to reach higher coordination numbers and thus achieve more options for the formation of bridging bonds to other metal ions and ultimately to form 3D arrangements.

The $C_2O_4^{2-}$ anion easily decomposes to the vapor phases CO_2 and CO, by the low-temperature routes, and hence, the oxalate-based solids could serve as a convenient source of oxides.[5] Because of their low thermal stability, the heterometallic oxalate complexes have already been used for the preparation of mixed metal oxides.[5−9] In our previous work, we reported the formation of the $Zn_3Nb_2O_8$ oxide phase, a preferred class of ceramic materials, by the thermal decomposition process of an oxalate-based compound of zinc(II) and niobium(V).[4] In general, the method of obtaining oxide materials through the thermal decomposition of well-defined single-source precursors, as compared with conventional methods, has several advantages: (*i*) the obtained material is more homogeneous because the metals are mixed at the molecular level; (*ii*) the resulting materials have relatively high specific surface areas because the crystalline oxides are formed under significantly milder conditions than are those in, for instance, solid-state reaction processes; and (*iii*) there is a

Received: August 29, 2012
Published: February 4, 2013

   dx.doi.org/10.1021/ic301888p | *Inorg. Chem.* 2013, 52, 1832−1842

much greater control of the metal stoichiometry in the final oxide.[10−13]

Recent researches[14,15] on the multicomponent Nb-containing oxide materials revealed their very appealing structural and physical properties, which caused a great deal of interest in these systems and led to their development for a wide range of applications. Such oxides are, for example, widely investigated as ferroelectric and piezoelectric materials, as ion conductors, and also as promising catalysts in several highly challenging processes, like water photodecomposition, alkane oxidation, or ammoxidation.[11,16] Because of the growing need for these materials, further investigation of the Nb-containing heterometallic compounds that could serve as single-source molecular precursors for the preparation of the Nb-based oxides is of great importance. In this contribution, the newly prepared complex $\{Ba_2(H_2O)_5[NbO(C_2O_4)_3]HC_2O_4\}\cdot H_2O$ (**1**), obtained by the use of the $[NbO(C_2O_4)_3]^{3-}$ anions as building blocks toward barium(II) cations, is reported, and its spectroscopic, thermal and structural properties were investigated. We focused on the ability of compound **1** to act as a single-source precursor for the formation of mixed Ba^{II}−Nb^{V} oxides. Thermal processing of **1** resulted in the formation of the mixed-metal oxide phases, $Ba_4Nb_2O_9$ and $Ba_5Nb_4O_{15}$, taking place at different temperatures.

Recent investigation revealed that $Ba_4Nb_2O_9$ and $Ba_5Nb_4O_{15}$ exhibit mixed electronic, oxide ion and proton conduction, which makes them especially attractive in the field of fuel cells, steam electrolyzers, and humidity sensors.[16,17] Up till now, most of the $Ba_5Nb_4O_{15}$ oxide powders were prepared by conventional, high-temperature solid-state reaction processes,[18−22] hydrothermal methods,[17,23−25] sol−gel synthesis,[26] or by the molten salt synthesis route.[27] The $Ba_4Nb_2O_9$ oxide powders were prepared mostly by conventional, high-temperature solid-state reaction processes[16,28−30] or by the hydrothermal method, when the pH value was equal to or larger than 14.[25] The $Ba_4Nb_2O_9$ oxide can exist in several polymorphic modifications, the hexagonal α-modification, the high-temperature orthorhombic γ-modification, and the closely related β-modification.[31,32] A detailed investigation on the phase transitions in the $Ba_4Nb_2O_9$ system was performed by Bezjak et al.,[28−30] whereas the structures were solved and fully elucidated only recently by Ling et al.[16]

The heat treatment of compound **1** resulted in the isolation of three stable polymorphs of $Ba_4Nb_2O_9$: the known hexagonal α- and orthorhombic γ-$Ba_4Nb_2O_9$, and the hexagonal δ-$Ba_4Nb_2O_9$ polymorph that was not reported previously. Detailed structural study on these oxide materials together with their thermal stability and electrical properties are also reported.

Taking into account the new method for the preparation of mixed oxide materials via thermal decomposition of well-defined heterometallic complexes, the compound $\{Ba_2(H_2O)_5[NbO(C_2O_4)_3]HC_2O_4\}\cdot H_2O$ (**1**) represents a prospective and applicable precursor for the synthesis of mixed Ba^{II}−Nb^{V} oxides.

EXPERIMENTAL SECTION

Materials and Methods. All reactions were performed under ambient conditions. The chemical reagents Nb_2O_5 (99.5%, Alfa Aesar), $KHSO_4$ (p.a., Sigma-Aldrich), NH_4Cl (99.5%, Sigma-Aldrich), $H_2C_2O_4\cdot 2H_2O$ (99.5%, Kemika), $(NH_4)_2C_2O_4\cdot H_2O$ (p.a., Kemika), $Ba(NO_3)_2$ (p.a., Kemika) were commercial products, used without further purification. Elemental analysis for C and H in **1** was carried out using a Perkin-Elmer Model 2400 microanalytical analyzer. Infrared spectra were recorded as KBr pellets on a Bruker Alpha-T spectrometer in the 4000−350 cm^{-1} region. The thermogravimetric analysis (TGA) data were collected on a Shimadzu DTG-60H analyzer, in the range from room temperature (RT) to 1500 °C, in the stream of synthetic air, at a heating rate of 10 °C min^{-1}. Differential scanning calorimetry (DSC) analyses were performed on a Mettler-Toledo TGA/DSC Star 1 System in the range from RT to 1200 °C, in air, at a heating/cooling rate of 10 °C min^{-1}.

Synthesis of $(NH_4)_3[NbO(C_2O_4)_3]\cdot H_2O$. A melt obtained by fusing Nb_2O_5 (2.01 g, 7.56 mmol) with $KHSO_4$ (10.0 g, 73.6 mmol) in a Pt-crucible[33,34] was dissolved, after cooling, in a 2% aqueous solution (200 mL) of $H_2C_2O_4\cdot 2H_2O$ (4.00 g, 31.7 mmol) by heating on a water bath. From the clear solution, $Nb(OH)_5\cdot nH_2O$ was precipitated by addition of a 12% aqueous solution of ammonia, until pH > 7. The precipitate was washed four times, every time with ∼40 mL of a 2% aqueous solution of NH_4Cl (4.00 g, 74.8 mmol; 200 mL), to remove SO_4^{2-} ions, and then dissolved in 200 mL of a 3% aqueous solution of $H_2C_2O_4\cdot 2H_2O$ (6.00 g, 47.6 mmol). The process of precipitation and rinsing of $Nb(OH)_5\cdot nH_2O$ was repeated once more, and the precipitate was finally dissolved in 100 mL of an aqueous solution of $H_2C_2O_4\cdot 2H_2O$ (5.11 g, 40.5 mmol; 50 mL) and $(NH_4)_2C_2O_4\cdot H_2O$ (3.01 g, 21.2 mmol; 50 mL). During the reduction of the volume of the obtained solution, by heating on the water bath, an excess of oxalic acid set aside, which was removed by filtration and the clear solution was left to evaporate at ambient conditions. (If formed again during the evaporation process, the crystals of $H_2C_2O_4\cdot 2H_2O$ were subsequently removed from the solution). The pH value of the final solution was adjusted to pH = 4 using a 12% aqueous solution of ammonia. In a one-week period, from this highly concentrated solution, colorless stick-like single crystals of $(NH_4)_3[NbO(C_2O_4)_3]\cdot H_2O$[35] formed. The yield was 1.75 g (26.0%). The analytical data of the obtained stick-like crystals had analytical data consistent with the literature report.[35]

Synthesis of $\{Ba_2(H_2O)_5[NbO(C_2O_4)_3]HC_2O_4\}\cdot H_2O$ (1). To an aqueous solution (15 mL) of $(NH_4)_3[NbO(C_2O_4)_3]\cdot H_2O$ (0.552 g, 1.24 mmol) an aqueous solution (15 mL) of $Ba(NO_3)_2$ (0.638 g, 2.44 mmol) was added dropwise with stirring at RT. The colorless stick-like single crystals of **1** formed in the solution within 24 h. The reaction beaker was then tightly closed and left for one more day, when the crystals were separated from the mother liquid, washed with water, and dried in air for 2 h. The yield was 0.684 g (65.1%). Anal. Calcd for $C_8H_{13}Ba_2NbO_{23}$: C, 11.37; H, 1.55. Found: C, 11.42; H, 1.60. IR, cm^{-1}: 3618 (m), 3470 (s, br), 2925 (w), 1749 (s), 1709 (vs), 1687 (vs), 1660 (vs), 1603 (s), 1409 (s), 1385 (s), 1308 (m), 1280 (sh), 1257 (m), 935 (m), 915 (m), 851 (w), 808 (m), 750 (w), 730 (w), 598 (sh), 570 (sh), 549 (m), 524 (w), 483 (m), 381 (m).

X-ray Single-Crystal Study. The X-ray data for the single crystal of compound **1** were collected at RT by ω-scans on an Oxford Diffraction Xcalibur 3 CCD diffractometer with a graphite-monochromated Mo$K\alpha$ radiation (λ = 0.71073 Å). Data reduction was performed with the CrysAlis PRO software package.[36] The structure was solved using SHELXS97[37] and refined with SHELXL97.[37] The model was refined using the full-matrix least-squares refinement; all non-hydrogen atoms were refined anisotropically. Hydrogen atoms were located in a difference Fourier map and refined as mixed, free, and riding entities. Molecular geometry calculations were performed by PLATON,[38] and molecular graphics were prepared using ORTEP-3,[39] CCDC-Mercury,[40] and VESTA.[41] Crystallographic and refinement data for the structure of **1** reported in this paper are shown in Table 1.

Crystallographic data for the complex can be obtained free of charge via www.ccdc.cam.ac.uk/conts/retrieving.html (or from the Cambridge Crystallographic Data Centre, 12, Union Road, Cambridge CB2 1EZ, U.K.; fax: +44 1223 336033; or deposit@ccdc.cam.ac.uk). CCDC 882329 contains the supplementary crystallographic data for this paper.

Thermal Synthesis of the Mixed Ba^{II}−Nb^{V} Oxides. Finely ground crystalline powders of compound **1** were pressed into compact pellets (12 mm in diameter and 2 mm in thickness) under 10000 kg/

dx.doi.org/10.1021/ic301888p | Inorg. Chem. 2013, 52, 1832−1842

Table 1. Crystallographic Data and Structure Refinement Details for Compound 1

	1
empirical formula	$C_8H_{13}Ba_2NbO_{23}$
formula wt./g mol^{-1}	844.74
space group	*Pnma*
a/Å	16.5679(6)
b/Å	11.6568(4)
c/Å	10.5831(4)
Z	4
V/Å^3	2043.90(13)
D_{calc}/g cm^{-3}	2.742
μ/mm^{-1}	4.477
Θ range/deg	4.16 − 32.64
range of h, k, l	$-19 < h < 24$
	$-16 < k < 7$
	$-15 < l < 9$
reflections collected	10385
independent reflections	3554
observed reflections ($I \geq 2\sigma$)	2907
R_{int}	0.0240
R (F), R_w (F^2)	0.0243, 0.0564
goodness of fit	0.972
H atom treatment	mixed
no. of parameters, restraints	190, 11
$\Delta\rho_{max}$, $\Delta\rho_{min}$ (e Å^{-3})	0.947; −0.759

cm^2, placed in an Al_2O_3 boat crucible, and heated in a furnace (Nabertherm, model LHT 04/17) to a certain temperature, in the range 600−1500 °C, in air, with a constant rate of 3 °C min^{-1}. At a selected temperature the resulting materials were held for 3 h and then cooled down to RT with a cooling rate of 3 °C min^{-1}. In each thermal treatment two compact pellets were heated simultaneously. Upon cooling, one heat-treated pellet was pulverized into fine powder using an agate mortar and a pestle, and analyzed by the X-ray powder diffraction, whereas the other pellet was used for electrical characterization.

X-ray Powder Structural and Microstructural Study. X-ray powder diffraction (XRD) patterns were measured in the reflection mode with the monochromated CuKα radiation (λ = 1.54179 Å) on a Philips diffractometer PW1830. Rietveld refinement was performed by the HighScore Xpert Plus program (Panalytical) and Topas Academic. Based on the choice of structural model, as well as on the type of profile function, the program simulates the XRD patterns and compares them with the experimental ones in the least-squares comparison mode. Thus, a certain number of least-squares structural and profile parameters were refined. Diffraction profiles were described by the Pseudo-Voigt function. A polynomial model was used to describe the background. Five background parameters, a scale factor, a zero-point shift, half-width parameters (U, V, W), peak shape parameters, and asymmetry parameters, were included in the refinement. Structural parameters, atomic coordinates, and B_{iso} were also refined unless, in some cases depending on specific circumstances, they needed to be constrained. Indexing and space group determination for unknown phase was carried out using the N-TREOR09 implemented in the EXPO2010 program.[42] Following the procedure of indexing, the space group determination was done by using statistics of the normalized z intensities (as extracted by the Le Bail method) to calculate the probability of each extinction symbol compatible with the crystal system suggested by N-TREOR09. Microstructural information was obtained during the Rietveld refinement in Topas Academic utilizing the Double-Voigt approach.[43] The LaB_6 powder was used as an instrumental broadening standard. Diffraction profiles for both the sample and the standard were described by the TCHZ-type Pseudo-Voigt function. Molecular graphics were prepared using VESTA.[41]

Electrical Characterization. Electrical conductivity of heat treated samples was measured by impedance spectroscopy (Novocontrol Alpha-N dielectric analyzer) in the frequency range 0.01 Hz−3 MHz and in the temperature range 30−240 °C. For the electrical contact, gold electrodes 8 mm in diameter were sputtered onto both sides of the sample discs using the SC7620 Sputter Coater, Quorum Technologies. All measurements were performed in heating and subsequent cooling in nitrogen atmosphere. The impedance spectra were analyzed by equivalent circuit modeling using the complex nonlinear least-squares fitting procedure (ZView software). Selected samples were also examined by DC conductivity measurements. The conductivity of the samples was measured as a function of temperature in heating from RT to 490 °C and subsequent cooling to RT in nitrogen atmosphere. The heating and cooling rates were 10 °C min^{-1} and the applied voltage was 100 V. The resulting current was measured using a digital electrometer (Keithley 6514).

RESULTS AND DISCUSSION

I. Characterization of Complex 1. The title compound (**1**) was obtained in the form of colorless stick-like crystals from an aqueous solution containing the $[NbO(C_2O_4)_3]^{3-}$ and Ba^{2+} entities in the molar ratio 1:2. The novel, air-stable and water-soluble, heterobimetallic complex of barium(II) and niobium(V) was characterized and tested for thermolytic conversion to oxide materials.

Molecular and Crystal Structure. The molecular structure of **1** consists of two Ba^{2+} cations, one $[NbO(C_2O_4)_3]^{3-}$ anion, and one $HC_2O_4^-$ anion, together with six water molecules. The Ba and Nb atoms and one of the three $C_2O_4^{2-}$ anions bonded to Nb are located in a crystallographic mirror plane (p.p. 0.5); another $C_2O_4^{2-}$ anion is located in a general position (p.p. 1.0). In addition, a half of the $HC_2O_4^-$ anion is also present, disordered about an inversion center (its centroid, i.e., midpoint of the C5−C5 bond, is located in the inversion center, therefore p.p. 0.5), as well as three molecules of water of crystallization, two of them being located in a general position (p.p. 1.0) and two halves in a mirror plane (p.p. 0.5).

The niobium(V) atom is heptacoordinated by seven O atoms forming a distorted pentagonal bipyramid (Figure 1; Supporting Information, Table S1). The oxo-oxygen atom (O11) is located in the apical position of the pentagonal bipyramid forming the shortest bond with the niobium atom (Nb1−O11 = 1.722(2) Å; Supporting Information, Table S1). The other apical position of the coordination polyhedron around Nb1 is occupied by the oxygen (O2) atom from the $C_2O_4^{2-}$ group; in its equatorial plane lie O1 of the same anion and two $C_2O_4^{2-}$

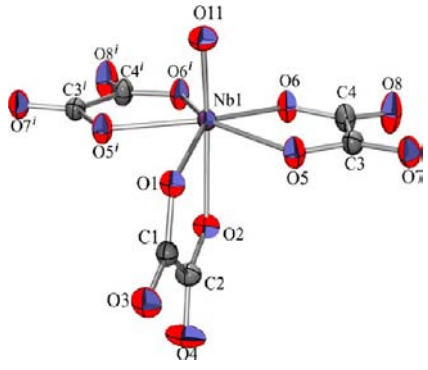

Figure 1. ORTEP-3[39] drawing of the coordination sphere of the Nb atom. Atomic displacement ellipsoids are drawn at the 50% probability level. Symmetry operator: (i) x, 1/2 − y, z.

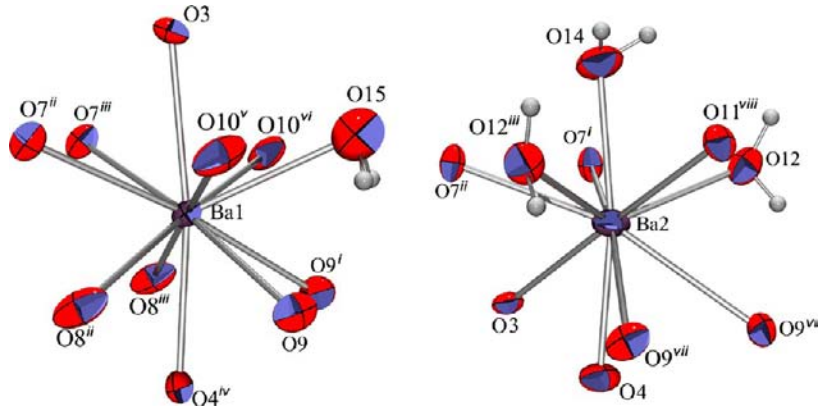

Figure 2. ORTEP-3[39] drawing of the coordination spheres of the Ba atoms. Atomic displacement ellipsoids are drawn at the 50% probability level and H atoms are shown as spheres of arbitrary radii. Symmetry operators: (*i*) $x, 1-y, z$; (*ii*) $-1/2+x, 1/2+y, -1/2+z$; (*iii*) $1/2-x, -y, -1/2+z$; (*iv*) $1/2+x, 1/2-y, -5/2+z$; (*v*) $-x, -1-y, 2-z$; (*vi*) $-x, -1/2+y, -2-z$; (*vii*) $x+1/2, y, -5/2-z$; (*viii*) $x, y, 1-z$.

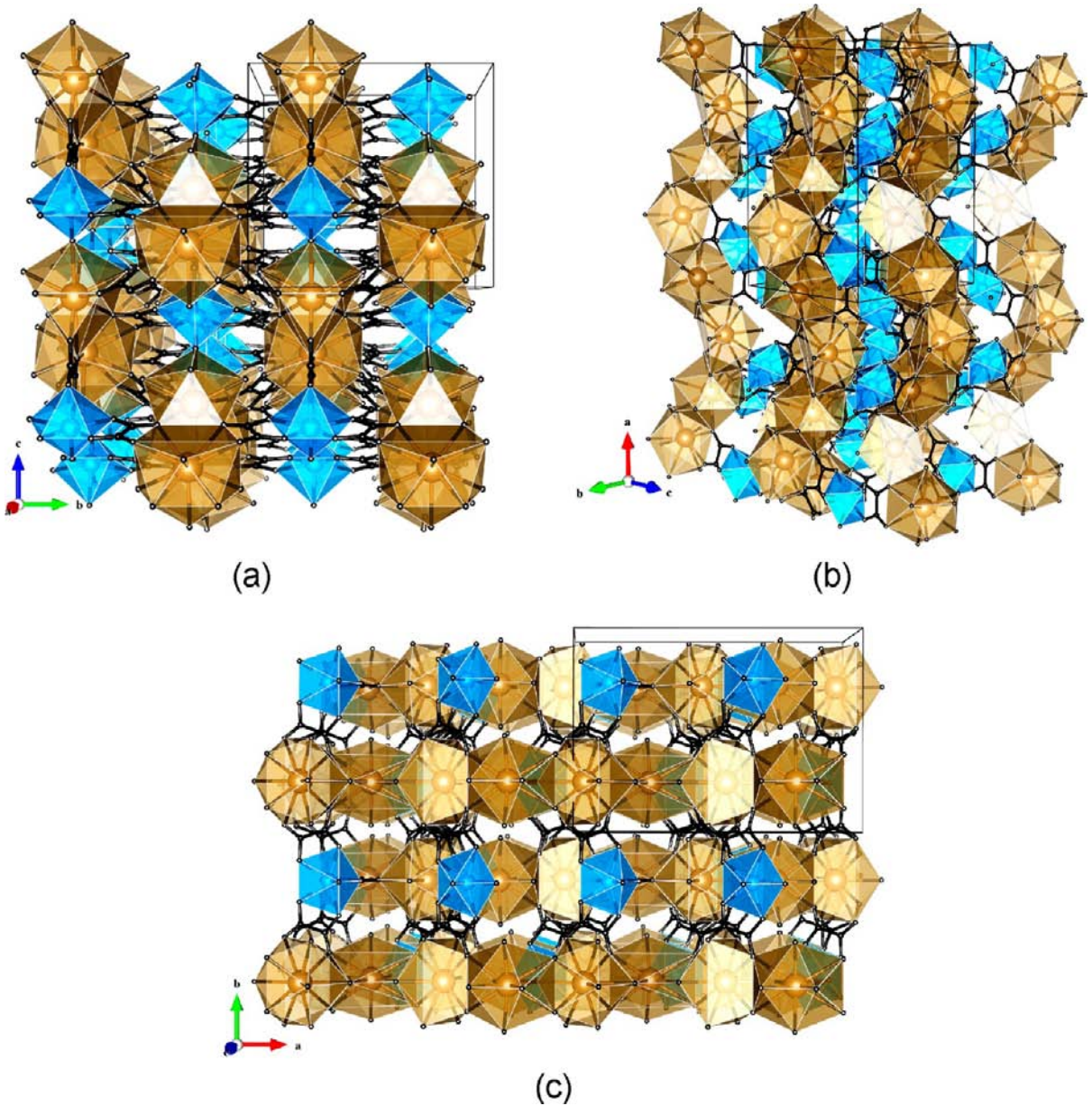

Figure 3. Crystal packing of compound **1** viewed in the directions (a) [100], (b) [01$\bar{1}$], and (c) [001]. The coordination spheres of the Nb and Ba atoms are depicted as blue and golden-brown polyhedra, respectively.

dx.doi.org/10.1021/ic301888p | *Inorg. Chem.* 2013, 52, 1832−1842

anions mutually related by the mirror plane (Figure 1). Generally, the conformation of the tris(oxalato)oxoniobate(V) anion in **1** is practically the same as that found in the compounds $(NH_4)_3[NbO(C_2O_4)_3]\cdot H_2O$[35] or $Rb_3[NbO(C_2O_4)_3]\cdot 2H_2O$.[44]

One Ba atom, Ba1, is surrounded by six O atoms from four $C_2O_4^{2-}$ groups and four O atoms from $HC_2O_4^-$ groups. It is also linked to one water molecule, reaching a coordination number of 11. Ten O atoms are coordinated to the Ba2 cation, four of them belonging to three $C_2O_4^{2-}$ ligands, two to two $HC_2O_4^-$ anions, three to water molecules, and one to the oxo-oxygen atom. The environments of the Ba cations are shown in Figure 2, and the corresponding interatomic distances and angles are given in Supporting Information, Tables S2 and S3.

The values of the Ba−O bond distances vary between 2.681(3) and 3.187(2) Å (Supporting Information, Tables S2 and S3), and can be regarded as a borderline case between covalent and ionic. The sum of covalent radii of the Ba and O atoms is 2.81 Å.[45] However, it is difficult to determine a definite cutoff parameter for such a large and easily polarizable cation. The mean length of the Ba−O contacts from the Cambridge Structural Database (including those listed as bonds) is 2.82(10) Å;[1] the majority fall within the range 2.75−2.90 Å. The irregularity of the Ba coordination polyhedra (Figure 2) does not indicate localized, directional bonds that could be regarded as covalent, regardless of the Ba−O distances. Therefore, compound **1** can be viewed either as an ionic compound (comprising discrete Ba^{2+} cations) or as a metal-coordinated framework. Given that the present definitions of both are rather vague, we will refrain from a definite answer.

The crystal packing of **1** reveals a complex 3D network, which comprises a coordination framework with niobium and barium (Figure 3) and a clathrate-like 3D hydrogen-bonding network (Supporting Information, Figure S1). Within the coordination framework, the Nb polyhedron is connected to eight neighboring Ba polyhedra through the $C_2O_4^{2-}$ ligands and the oxo-oxygen group whereas the Ba polyhedra share edges and vertices (Figures 4). Finally, a cage is formed around metal cations and a non-hydrogen-bonded $C_2O_4^{2-}$ anion (C1−C2) (Supporting Information, Figure S1, and Table S3).

Thermal Analysis. Thermal behavior of the title compound has been studied by the thermogravimetric analysis (TGA) performed on a crystalline sample in synthetic air, up to 1500 °C. The corresponding curve is presented in Figure 5, and the thermoanalytical data are summarized in Table 2. The elimination of six water molecules proceeds in two, not very well separated steps that take place over the temperature range of 32−265 °C (exp. 12.47%; calcd. 12.80%). In the first step, up to 98 °C, two water molecules are expelled, and the remaining four water molecules are lost over a wider temperature interval. The main loss of mass (34.88%) takes place in the temperature range of 265−875 °C, with three close, but still discrete steps in the TGA curve. The first two of the three steps, from 265 to 645 °C, could be associated with the removal of $4CO_2$ and 3CO (exp. 31.25%; calcd. 30.79%). The loss of the remaining CO takes place in the next step from 645 to 875 °C (exp. 3.63%; calcd. 3.32%). The mass of a white-colored residue which corresponds to the mixture of 2BaO and $1/2Nb_2O_5$ (exp. 52.21; calcd. 52.03%) is constant up to 1150 °C. The loss of mass is 0.093% up to 1500 °C.

Infrared Study. In the IR spectrum of complex **1** absorption bands that can be attributed to the vibrations of the $C_2O_4^{2-}$ groups, oxo-oxygen atom, and water molecules are present. The band of medium intensity in the 3650−3200 cm^{-1} region originates from the O−H stretching vibration [ν(OH)] of water molecules and $HC_2O_4^-$ anion. The relatively strong absorption bands corresponding to coordinated $C_2O_4^{2-}$ groups are located at 1709, 1687, and 1660 cm^{-1} [ν_{as}(CO)], 1409, 1257, and 915 cm^{-1} [ν_s(CO)] and 808 cm^{-1} [δ(OCO)].[2,44,46] A medium-intensity absorption band at 936 cm^{-1} could be recognized as ν(Nb=O).[2−4,44]

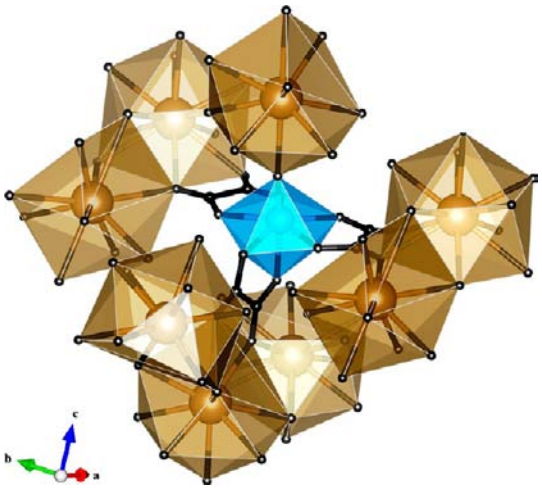

Figure 4. Environment of the Nb polyhedron: it is linked to seven Ba polyhedra through the bridging $C_2O_4^{2-}$ groups, and to one Ba polyhedron through the oxo-oxygen group in the vertex-sharing fashion. The orientation of the Nb polyhedron is the same as in Figure 1.

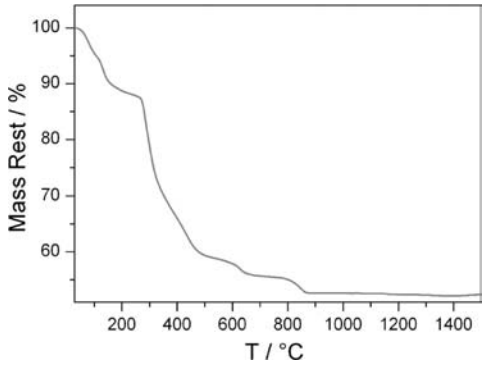

Figure 5. TGA curve of compound **1** measured in the synthetic air atmosphere.

Table 2. Thermoanalytic Data for Compound 1

		weight loss/%		
compound	T_1-T_2/°C	exp.	calcd.	loss
1	32−265	12.47	12.80	$-6H_2O$
	265−645	31.25	30.79	$-4CO_2$, −3CO
	645−875	3.63	3.32	−CO

II. Characterization of the Mixed Ba^{II}−Nb^{V} Oxides. Finely ground crystalline powders of compound **1** were pressed into compact pellets and heated up to the selected temperatures in the range 600−1500 °C, and then cooled to RT. The heating/cooling rate was 3 °C min^{-1}, and the holding time was 3 h at each temperature. To check possible influence of pressure on the composition of the oxides obtained by heating compound **1** at selected temperatures, two samples, powdered

dx.doi.org/10.1021/ic301888p | Inorg. Chem. 2013, 52, 1832−1842

and compacted, were heated. The phase composition of the samples obtained at the same temperature in two different ways (powder and compact pellets) was the same.

Structural and Microstructural Study. Different nanocrystalline products obtained by pyrolysis of metal-complex precursor **1** in the range 600−1500 °C were explored by X-ray powder diffraction at RT. The X-ray powder patterns of the selected products are displayed in Figure 6.

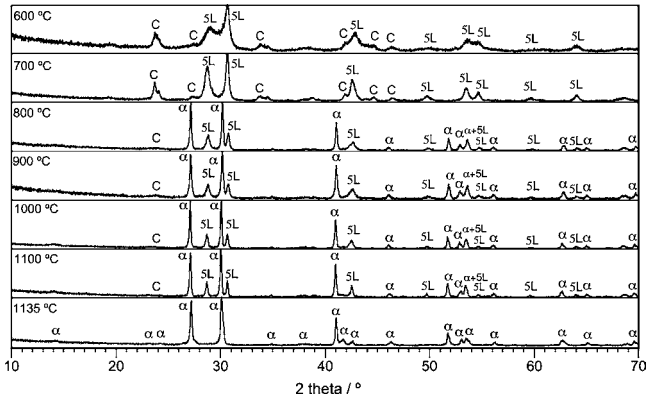

Figure 6. X-ray diffraction patterns of samples obtained by heating compound **1** up to the indicated temperatures and cooling to RT. The heating/cooling rate was 3 °C min^{-1}, and the holding time was 3 h at each temperature. The diffraction lines indicated by C belong to $BaCO_3$, whereas the lines indicated by α and 5L belong to α-$Ba_4Nb_2O_9$ and $Ba_5Nb_4O_{15}$, respectively.

In the pattern of the product prepared by heating compound **1** at 700 °C for 3 h, the majority of diffraction lines were indexed and attributed to the hexagonal $Ba_5Nb_4O_{15}$ phase (indicated as 5L in Figure 6), but also a small amount of an additional phase, $BaCO_3$ (indicated as C in Figure 6), was observed. In **1**, the molar ratio Ba:Nb is 2:1, whereas in $Ba_5Nb_4O_{15}$, the Ba:Nb molar ratio is 1.25:1, which unavoidably results in the formation of the additional Ba-consisting phase, $BaCO_3$. A quantitative analysis by the Rietveld method revealed that the product contains 70.4(3) wt % of $Ba_5Nb_4O_{15}$ and 29.6(1) wt % of $BaCO_3$. Similar composition was found for the product prepared at even lower temperatures, by heating **1** at 600 °C for 3 h, but broad and unresolved diffraction lines indicated very small crystallite sizes at that point (Figure 6).

Thermal treatment of **1** at 800 °C for 3 h led to the formation of the hexagonal α-$Ba_4Nb_2O_9$ polymorph (indicated as α in Figure 6), with a reduction of the $Ba_5Nb_4O_{15}$ and $BaCO_3$ phases in the mixture. The sample obtained at this temperature contained 81.5(9) wt % of α-$Ba_4Nb_2O_9$, 15.1(7) wt % of $Ba_5Nb_4O_{15}$, and 3.9(5) wt % of $BaCO_3$. Products obtained at higher temperatures, by heating compound **1** at 900 °C, 1000 °C, and 1100 °C, have the same composition, within the standard deviations, as the one described above (Figure 6).

The heating of complex **1** for 3 h at 1135 °C produced the hexagonal polymorph of $Ba_4Nb_2O_9$, the α-$Ba_4Nb_2O_9$ phase, with no additional phases present. The α-$Ba_4Nb_2O_9$ phase crystallizes in the $P\bar{6}2c$ space group with the unit-cell parameters a = 10.2403(2) Å and c = 8.4767(2) Å. In relation to these values, the parameters of the hexagonal cell found by Leschenko et al.[31,32] are $(3a)^{1/2}$ and $1/2c$, respectively, whereas the values reported by Ling et al.[16] are slightly bigger.

The structure obtained by Ling et al.[16] was used as a starting structural model in the Rietveld refinement of the X-ray data of the product obtained at 1135 °C. The graphical result of this refinement is shown in Figure 7; good agreement of the observed and calculated patterns unambiguously confirms the formation of α-$Ba_4Nb_2O_9$ at the indicated temperature.

A line-broadening analysis was undertaken to extract precise microstructural information on α-$Ba_4Nb_2O_9$ from the XRD patterns of the products obtained at the selected temperatures, from 800 to 1135 °C (Table 3). The α-$Ba_4Nb_2O_9$ phase could be characterized as a strain-free phase. The calculated lattice strain for all the samples was e = 0%; therefore, the strain is omitted from the table. It was noticed that the volume-weighted domain lengths $\langle L\rangle_V$ for α-$Ba_4Nb_2O_9$ are dependent on the heat treatment applied to **1**. The values of $\langle L\rangle_V$ were around 100 nm for the samples prepared in the temperature

Table 3. Volume-Weighted Domain Lengths of α-$Ba_4Nb_2O_9$ Phase Obtained at Different Temperatures

T/°C	$\langle L\rangle_V$/nm
800	113
900	100
1000	98
1100	95
1135	43

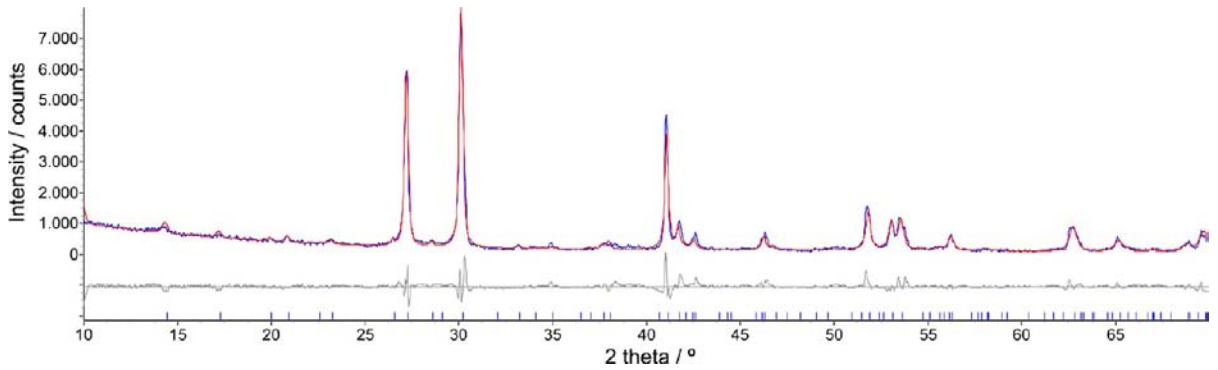

Figure 7. Graphical result of the final Rietveld refinement of RT data for α-$Ba_4Nb_2O_9$, obtained by heating compound **1** at 1135 °C for 3 h followed by cooling to RT. The blue vertical marks represent the positions of α-$Ba_4Nb_2O_9$. Experimental data are shown in blue, the calculated pattern in red, and the difference curve is gray.

dx.doi.org/10.1021/ic301888p | *Inorg. Chem.* 2013, 52, 1832−1842

range 800−1100 °C, whereas $\langle L \rangle_V$ decreased to 43 nm at 1135 °C, when the sample consisted of α-$Ba_4Nb_2O_9$ exclusively.

The heat treatment of molecular precursor **1** at 1175 °C and the cooling to RT resulted in the crystallization of another two polymorphs of $Ba_4Nb_2O_9$. The major component was γ-$Ba_4Nb_2O_9$, a long-known polymorph but structurally totally abstruse until recently, when it was elucidated by the Ling's group.[16] Based on a density functional theory (DFT) geometry optimization and the refinement against the single-crystal X-ray and powder neutron data, they proposed an "average" structure for γ-$Ba_4Nb_2O_9$, emphasizing that the structure published is only a subcell of a well-ordered monoclinic supercell containing several hundred independent atoms. This structure was used as our starting model for the Rietveld refinement. All unit-cell parameters together with the profile function parameters were refined but, because of the complexity of the structure vs a deficiency of the experimental XRD data, atomic coordinates were constrained to the values found by Ling et al.[16] The strategy resulted in a more than satisfactory fit (bearing in mind the very heavy constrained refinement) of the γ-$Ba_4Nb_2O_9$ structure to our experimental data; however, it became obvious that an additional phase exists because there were a number of diffraction lines that could not be attributed to the γ polymorph. All these lines were indexed in the hexagonal space group $P6_3/m$ with the unit-cell parameters a = 5.9002(9) Å and c = 14.811(1) Å.

The attempts to solve the structure from the XRD data by direct methods failed, mostly because this polymorph was a minor phase in the mixture [only 18.5(5) wt %]. As an alternative, an exhaustive search of known structures in chemically related systems was undertaken. On this basis, we determined that the new phase adopts the 6H-perovskite structure type. Unlike the ideal $BaTiO_3$ which belongs to $P6_3/mmm$, this structure crystallizes in the reduced-symmetry space group $P6_3/m$, caused by the effective ionic-radii size mismatch between the B-site cations in the 6H-perovskite structure type. The structure is closely related to those of $Ba_3SrNb_2O_9$[47] and γ-$Ba_4Ta_2O_9$.[48] We named the new phase *delta*, δ-$Ba_4Nb_2O_9$, whose crystal structure is shown in Figure 8. Fractional atomic coordinates and thermal parameters for δ-$Ba_4Nb_2O_9$ are given in Table 4, whereas the crystal data and a summary of the structure refinement are presented in Table 5. The structure consists of the $Nb_2O_9^{8-}$ face-sharing octahedral dimers which are interconnected via corners to the regular BaO_6^{10-} octahedra. There are two additional crystallographically different Ba atoms in the asymmetric unit. The Ba1 atom is coordinated by three O2 atoms in two adjacent layers and two groups of three O1 atoms in the same layer, achieving the coordination number 12. The Ba2 atoms are surrounded by three O1 atoms in an adjacent layer, by two groups of three O2 atoms in the same layer, and by three O2 atoms in the other adjacent layer. Selected bond distances and angles for δ-$Ba_4Nb_2O_9$ are given in Table 6. A quantitative analysis with a simultaneous determination of the crystallite size and lattice strain by the Rietveld method revealed that the product obtained by heating **1** at 1175 °C contains 81.5(4) wt % of γ-$Ba_4Nb_2O_9$ and 18.5(5) wt % of δ-$Ba_4Nb_2O_9$, with the average crystallite sizes 38 and 29 nm, respectively. The lattice strain was e = 0.04% for γ-$Ba_4Nb_2O_9$ and negligibly small for δ-$Ba_4Nb_2O_9$. The graphical result of the final Rietveld refinement of the product obtained at 1175 °C is displayed in Figure 9.

Thus, the described synthesis route with the heating of **1** to 1175 °C gave rise to a mixture of the two polymorphs, γ- and δ-$Ba_4Nb_2O_9$, both existing at RT. In previous studies, it was found that the γ polymorph was metastable at RT and so could be isolated only by quenching the sample from high temperatures, because slow cooling (over several hours) led to a transformation to α-$Ba_4Nb_2O_9$.[31,32] Bezjak et al.[28−30] found that during the cooling process γ polymorph could be, as well, transformed to β-modification under specific cooling rate conditions (typically found after heating the quenched γ-phase from RT to ∼300 °C). Therefore, we also checked whether the diffraction lines could be assigned to the β phase according to PDF 35-1155;[31,32] however, no match was observed.

The DSC curve recorded during the process of heating **1** from RT to 1200 °C and cooling back to RT, is given in Figure 10. The curve obtained at cooling exhibits two maxima. The first exothermic effect at ∼1150 °C is associated with a reversible process of the $\alpha \leftrightarrow \gamma$ phase transition and is in agreement with those noted by Ling[16] and Bezjak.[28−30] However, we observed an additional exothermic signal at 610 °C (inset in Figure 10), likely caused by the formation of the δ phase. The appearance of both γ and δ polymorphs at RT, produced by cooling, indicates that only a partial $\gamma \rightarrow \alpha$

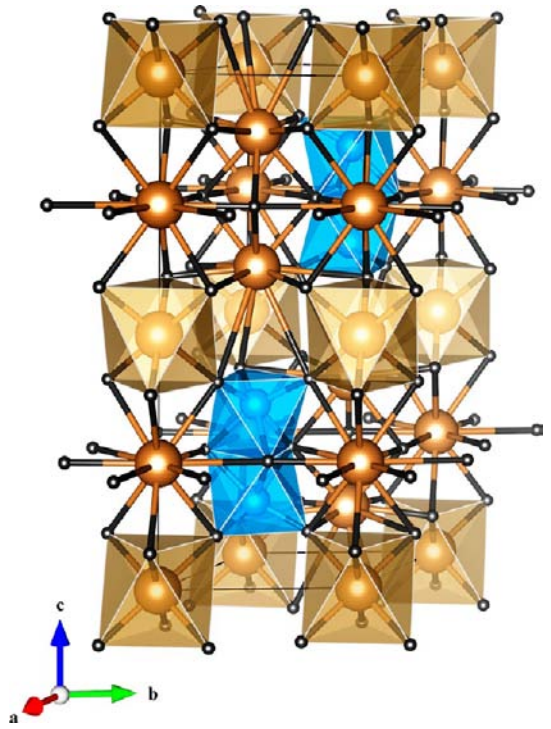

Figure 8. Crystal structure of the δ-$Ba_4Nb_2O_9$ phase. The polyhedron around the Nb atom is given in blue color. The coordination sphere of the Ba3 atom is depicted as the discrete golden-brown octahedron. The dodecahedra around the Ba1 and Ba2 atoms are omitted for clarity.

Table 4. Fractional Atomic Coordinates and Thermal Parameters for δ-$Ba_4Nb_2O_9$

atom	Wyck.	x	y	z	B_{iso}/Å^3
Ba1	2a	0.0000	0.0000	0.2500	0.4(2)
Ba2	4f	0.3333	0.6667	0.096(4)	0.5(1)
Ba3	2b	0.0000	0.0000	0.0000	0.7(2)
Nb1	4f	0.3333	0.6667	0.816(3)	0.4(2)
O1	6h	0.5601(4)	0.0424(1)	0.2500	1.2(3)
O2	12i	0.7591(1)	0.6431(2)	0.0969(1)	1.6(4)

dx.doi.org/10.1021/ic301888p | Inorg. Chem. 2013, 52, 1832−1842

Table 5. Crystal Data and Summary of Structure Refinement for δ-$Ba_4Nb_2O_9$

	Phase: δ-$Ba_4Nb_2O_9$
formula sum	$Ba_{8.00}Nb_{4.00}O_{18.00}$
formula mass/g mol^{-1}	1758.255
density (calculated)/g cm^{-3}	6.5379
weight fraction/%	18.5(5)
space group (No.)	$P6_3/m$ (176)
lattice parameters	
a/Å	5.9002(9)
c/Å	14.811(1)
$V/10^6$ pm^3	446.51070
fitting mode	structure fit
profile function	pseudo Voigt
U	0.52(3)
V	0.544(1)
W	−0.08(1)
asymmetry parameter 1	0.00012(1)
peak shape parameter 1	0.6(2)
peak shape parameter 2	0.0019(1)
R (weighted profile)/%	4.4548
R (profile)/%	3.1071
GOF	1.4604

Table 6. Selected Bond Distances (Å) and Angles (deg) for δ-$Ba_4Nb_2O_9$

Selected Bond Distances	
Ba1−O1 × 3	2.60(1)
Ba1−O2 × 6	2.915(8)
Ba1−O1 × 3	3.187(3)
Ba2−O2 × 3	2.6210(6)
Ba2−O1 × 3	3.00(9)
Ba2−O2 × 3	3.2837(2)
Ba2−O2 × 3	3.290(5)
Ba3−O2 × 6	2.3455(7)
Nb1−O1 × 6	2.07(3)
Nb1−O2 × 3	1.81(1)
Nb1−Nb1	1.95(7)
Selected Angles	
O2−Nb1−O1	173.5(4)
Nb1−O1−Nb1	66.0(6)

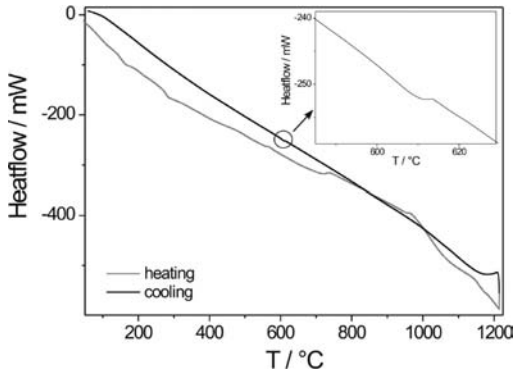

Figure 10. DSC curve (heating and cooling) for compound **1** measured in air.

transformation occurred, followed by an additional transition of the obtained α to the δ phase at ~600 °C.

To gain an insight into the products occurring at different stages of the cooling process, additional samples were prepared by heating compound **1**, followed by quenching, at 1200, 675, and 540 °C. A schematic illustration of the phases obtained in this way is given in Scheme 1. The heating of molecular precursor **1** at 1200 °C for 3 h and a sudden quenching to RT resulted in the formation of γ-$Ba_4Nb_2O_9$. However, the heating of compound **1** at 1200 °C for 3 h, cooling the sample to 675 °C, and then quenching, produced a mixture of γ and α phases. The quantitative Rietveld refinement of this sample yielded 79.8 wt % of γ-$Ba_4Nb_2O_9$ and 20.2 wt % of α-$Ba_4Nb_2O_9$, confirming a partial $\gamma \rightarrow \alpha$ transformation during the cooling. Applying the same procedure (heating at 1200 °C for 3 h and cooling) but quenching the sample at a temperature below the second signal in DSC, that is, at 540 °C, resulted in the occurrence of a polymorphic mixture consisting of γ and δ phases in the ~1:1/5 ratio, the same as in the originally investigated sample obtained by the slow cooling from 1175 °C to RT.

The mixture containing the γ + δ polymorphs, produced without quenching, simply by slow cooling from 1175 °C to RT, was characterized with a very small lattice strain (for both phases). For comparison, the structure of the γ phase produced by rapid quenching obviously contained certain lattice deformations, which yielded a strain value e = 0.13%.

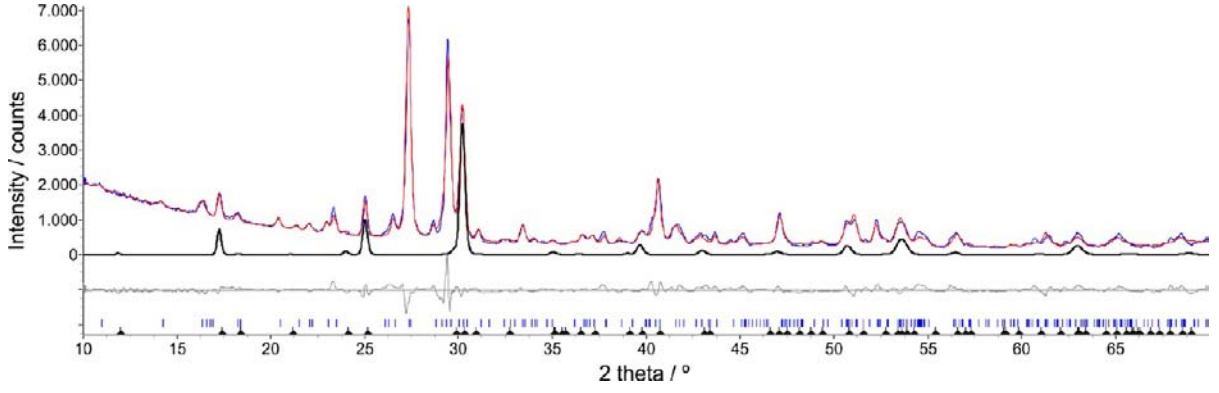

Figure 9. Graphical result of final Rietveld refinement on RT data for the mixture of two polymorphs, γ-$Ba_4Nb_2O_9$ and δ-$Ba_4Nb_2O_9$, obtained by heating compound **1** at 1175 °C followed by cooling to RT. Experimental data are shown in blue, the calculated pattern in red, and the difference curve in gray. Positions of diffraction maxima are given by vertical marks. For readership convenience the calculated diffraction pattern of the refined δ-$Ba_4Nb_2O_9$ phase is highlighted by the solid black line.

dx.doi.org/10.1021/ic301888p | Inorg. Chem. 2013, 52, 1832−1842

Scheme 1. Schematic Diagram of the $Ba_4Nb_2O_9$ Phases (γ-$Ba_4Nb_2O_9$, γ-$Ba_4Nb_2O_9$ + α-$Ba_4Nb_2O_9$, γ-$Ba_4Nb_2O_9$ + δ-$Ba_4Nb_2O_9$) Obtained at Different Temperatures during the Cooling Process, after Heating Molecular Precursor 1

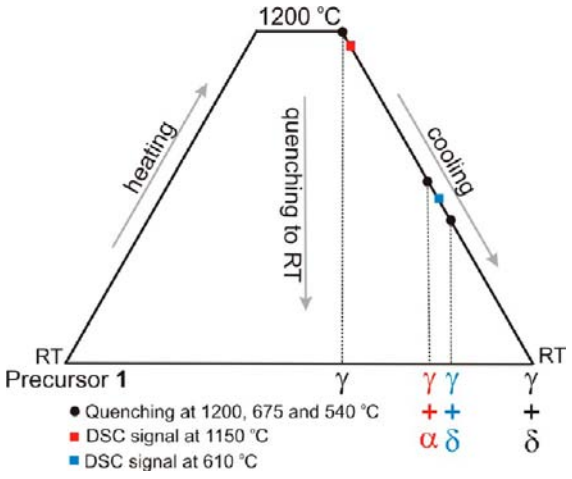

To furthermore establish relations, possible advantages or down faults, between the pathway employed for the synthesis of $Ba_5Nb_4O_{15}$ and $Ba_4Nb_2O_9$ and their properties, detailed conductivity measurements were performed on the samples heat treated for 3 h at 700, 800, 1135, and 1200 °C.

Electrical Characterization. Selected samples were investigated by impedance spectroscopy, and the impedance data were analyzed by means of equivalent circuit modeling. Typical complex impedance plots for all samples consist of a well-defined single arc as shown for the sample heated at 1200 °C in Figure 11. Ideally, the impedance semicircle passes through the origin of a complex plot and gives a low frequency intercept on the real axis corresponding to the resistance (R) of the sample. The equivalent circuit that represents such an ideal semicircle is a parallel combination of resistor (R) and capacitor (C). However, our experimental data show a depressed semicircle with the center below the real axis and in this case it is more appropriate to use a constant-phase element (CPE) instead of ordinary capacitor. Such nonideal behavior is common to many classes of materials and can be related to a heterogeneous property of a system, such as the presence of a distribution in relaxation times within the bulk response.[49]

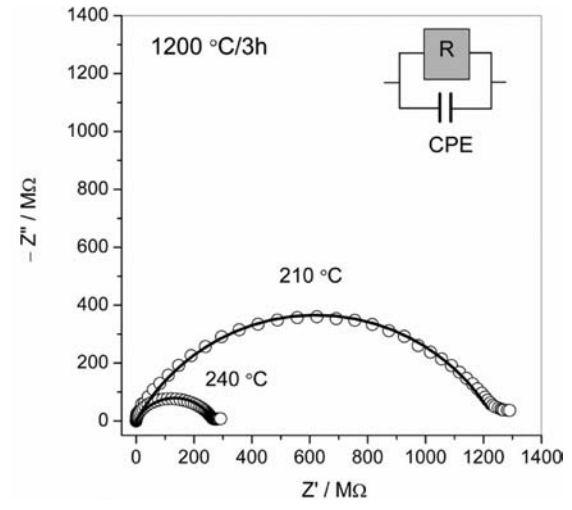

Figure 11. Complex impedance plots at 210 and 240 °C and the corresponding equivalent circuit for the crystalline phases obtained by heating of compound **1** at 1200 °C for 3 h. Circles denote experimental values; solid line corresponds to the best fit.

At each temperature, equivalent circuit modeling gives three parameters: bulk resistance (R) and two parameters for CPE. The values of bulk resistance, R, together with electrode dimensions (electrode area and sample thickness) were used to calculate total conductivity of the samples. The temperature dependence of total conductivity for the samples heated at 700 and 800 °C is presented in an Arrhenius plot in Figure 12.

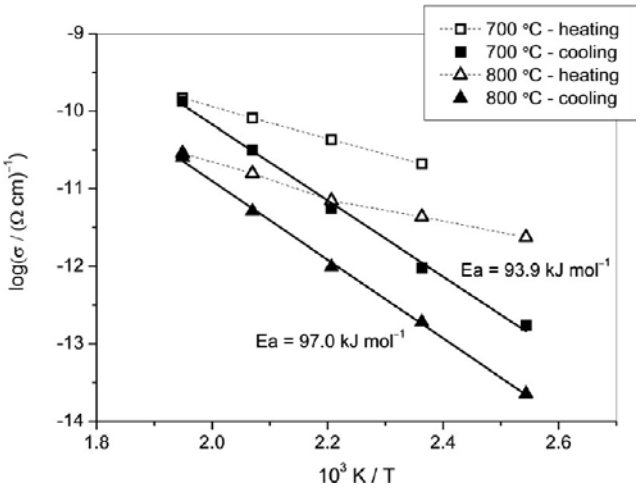

Figure 12. Temperature dependence of conductivity in heating and subsequent cooling in nitrogen for the crystalline phases obtained by heating of compound **1** at 700 and 800 °C. Solid lines represent the least-squares linear fits to experimental data, and dashed lines are drawn as guides for the eye.

Both samples exhibit a significant difference in conductivity measured in heating and subsequent cooling, which is related to the water absorbed in dominant crystalline phases. As already shown, thermal decomposition of compound **1**, heated at 700 °C for 3 h, led to the formation of $Ba_5Nb_4O_{15}$ [70.4(3) wt %] and $BaCO_3$ [29.6(1) wt %], whereas heating at 800 °C for 3 h resulted in the crystallization of three phases: α-$Ba_4Nb_2O_9$ [81.5(9) wt %], $Ba_5Nb_4O_{15}$ [15.1(7) wt %], and $BaCO_3$ [3.9(5) wt %]. The TGA studies revealed that $Ba_5Nb_4O_{15}$ and α-$Ba_4Nb_2O_9$ absorb significant amounts of water and gradually lose it on heating (Supporting Information, Figures S2 and S3). The proton conduction plays a leading role in the hydrated form of both phases; therefore, the conductivity measured in heating is considerably higher than the one in cooling. Also, the activation energies determined from the slope of $\log(\sigma)$ vs $1/T$ using the equation $\sigma = \sigma_O \exp(-E_a/k_BT)$ for partially dehydrated samples (cooling run) increase because of a decreasing contribution of protonic transport with a relatively low migration energy. The activation energies for partially dehydrated samples heated at 700 and 800 °C are very similar, 93.9 and 97.0 kJ mol^{-1}, respectively, and they are comparable to the activation energies of many niobates and oxide-ionic conductors.[16] The decrease in electrical conductivity for the sample heated at 800 °C for 3 h is caused by the crystallization of the less conductive α-$Ba_4Nb_2O_9$ phase on the account of the $Ba_5Nb_4O_{15}$ phase.

Electrical conductivity of the α-$Ba_4Nb_2O_9$ phase obtained by heating compound **1** at 1135 °C for 3 h is shown in Figure 13.

dx.doi.org/10.1021/ic301888p | Inorg. Chem. 2013, 52, 1832–1842

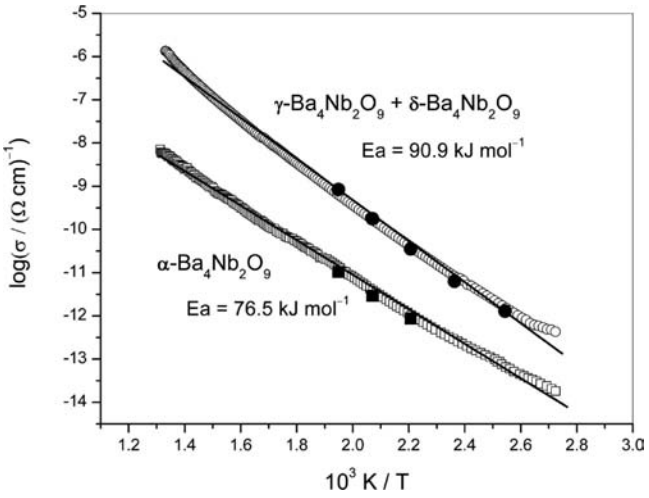

Figure 13. Temperature dependence of conductivity in cooling in nitrogen for the crystalline phase(s) obtained by heating of compound **1** at 1135 and 1200 °C. Open points represent the results from DC conductivity measurements, whereas solid points correspond to the data measured by impedance spectroscopy. Solid lines represent the least-squares linear fits to experimental data. The high conductivity values measured in heating are omitted from the figure.

To expand the limited temperature range of our experimental setup of impedance spectroscopy we applied DC conductivity measurements which allowed heating runs up to 490 °C. The values of conductivity obtained by these two techniques are in excellent agreement (Figure 13).

Taking into consideration possible differences in the microstructure which could have a strong impact on electrical properties, as well as only a partially overlapped temperature range of the conductivity measurements, the values of electrical conductivity of the α-$Ba_4Nb_2O_9$ phase obtained by thermal decomposition of **1** are comparable to the values reported by Ling et al.[16] (Table 7). According to their model, the dominant conduction in the hydrated α-$Ba_4Nb_2O_9$ is protonic, whereas at higher temperatures oxide ionic and electronic transports play an important role. Because the maximum temperature in our conductivity measurements was below the temperature of complete dehydration of α-$Ba_4Nb_2O_9$, it is expected that the migrations of protons and oxide ions control the conductivity in the reported temperature range (Figure 13). This is supported by the fact that the activation energy for conductivity for the partially dehydrated α-$Ba_4Nb_2O_9$ equals 76.5 kJ mol^{-1}, which is a value typical for ionic (proton and oxide ion migration) conduction.[16]

Table 7. Comparison of the Electrical Conductivity, σ_{DC}, of the Mixed-Metal Oxide Phases $Ba_5Nb_4O_{15}$ and $Ba_4Nb_2O_9$ Obtained in This Work with the Literature Data

phase	$\sigma_{DC}/(\Omega\ cm)^{-1}$	T/°C	measurement atmosphere	ref.
$Ba_5Nb_4O_{15}$ + $BaCO_3$	1.35×10^{-10}	250	N_2	this work
α-$Ba_4Nb_2O_9$	4.98×10^{-9}	470	N_2	this work
γ-$Ba_4Nb_2O_9$ + δ-$Ba_4Nb_2O_9$	1.11×10^{-6}	470	N_2	this work
$Ba_5Nb_4O_{15}$	$\sim 1.8 \times 10^{-8}$	300	N_2	17
α-$Ba_4Nb_2O_9$	$\sim 2.00 \times 10^{-7}$	580	dry 10% H_2 + 90% N_2	16
γ-$Ba_4Nb_2O_9$	$\sim 1.6 \times 10^{-7}$	470	dry Ar	16

The conductivity of the sample containing two polymorphs γ-$Ba_4Nb_2O_9$ and δ-$Ba_4Nb_2O_9$ (obtained by heating compound **1** at 1200 °C for 3 h) exhibits several orders higher conductivity, than the α-$Ba_4Nb_2O_9$ because of a faster protonic and oxide ionic transport in the gamma phase (Figure 13). In γ-$Ba_4Nb_2O_9$, protons from absorbed water occupy ordered positions in the structure, giving rise to a stoichiometric phase γ-$Ba_4Nb_2O_9 \times 1/3H_2O$ which partially dehydrates at ~490 °C.[16] The enhanced proton conduction in the hydrated γ-$Ba_4Nb_2O_9$ phase originates from the structural peculiarities: 2D layers containing Nb^{5+} cations with the low oxygen coordination number (4 or 5) separated by discrete OH groups that facilitate ionic transport. Most interestingly, the conductivity values of the mixture of 81.5(4) wt % of γ-$Ba_4Nb_2O_9$ and 18.5(5) wt % of δ-$Ba_4Nb_2O_9$ are similar to the ones of the pure γ-$Ba_4Nb_2O_9$ reported by Ling,[16] at least in the temperature range where the overlapping exists (Table 7). Although for a further conclusion it is necessary to investigate the transport properties of the pure δ-$Ba_4Nb_2O_9$ and take into consideration the influence of microstructure, this result suggests that the presence of ~20 wt % of δ-$Ba_4Nb_2O_9$ does not reduce overall conductivity of the sample controlled by highly conductive γ-$Ba_4Nb_2O_9$. Furthermore, it seems likely that δ-$Ba_4Nb_2O_9$ having the 6H-perovskite structure also exhibits significant water absorption capacity, crucial for high proton conduction, as structurally very similar γ-$Ba_4Ta_2O_9$.[48]

All these measurements were performed on samples that were prepared by pelleting powdered single crystals of complex **1** and heated to certain temperatures. The results of conductivity measurements are completely comparable with those reported by the Ling's group on $Ba_4Nb_2O_9$ ceramics, whose preparation included multiple reheating steps, typical for a conventional ceramics preparation procedure.[16] Therefore, the proposed synthetic procedure deserves additional attention because the benefit of a "two in one" approach—one-step preparation of the desired oxide phase that is already in a form suitable for conductivity measurements—is successfully established by this study.

CONCLUSIONS

A new heterobimetallic oxalate-based complex of barium(II) and niobium(V), $\{Ba_2(H_2O)_5[NbO(C_2O_4)_3]HC_2O_4\}\cdot H_2O$, was prepared and characterized from the structural, thermal, and spectroscopic point of view. Thermal decomposition of this single-source precursor provides mixed oxides, $Ba_5Nb_4O_{15}$ and $Ba_4Nb_2O_9$. Three stable $Ba_4Nb_2O_9$ polymorphs were isolated, already familiar hexagonal α- and orthorhombic γ-, and so far unknown hexagonal δ-$Ba_4Nb_2O_9$, having the 6H-perovskite structure. A polymorphic mixture containing γ-$Ba_4Nb_2O_9$ and δ-$Ba_4Nb_2O_9$ phases was isolated by slow cooling from 1175 °C to RT. Both phases were stable at RT, and this, according to previous studies, was unexpected. These results once again confirm that the mixed-metal oxides can originate from heterobimetallic oxalate complexes, which could serve as a convenient route for the preparation of technologically important materials.

Our further research would be related to the synthesis and characterization of novel oxalate complexes, especially to the compounds containing barium(II) and tantalum(V) ions, that are expected to have similar properties as the one reported here.

dx.doi.org/10.1021/ic301888p | Inorg. Chem. 2013, 52, 1832−1842

■ ASSOCIATED CONTENT

Supporting Information

Full geometry of the coordination spheres of the metal atoms, 3D clathrate-like hydrogen bonding network, the geometric parameters of hydrogen bonds, the TGA curves of obtained mixed Ba^{II}–Nb^{V} oxides. X-ray crystallographic file (CIF). This material is available free of charge via the Internet at http://pubs.acs.org.

■ AUTHOR INFORMATION

Corresponding Author

*Phone: +385 1 4561-189 (M.J.), +385 1 4561-189 (P.P.). Fax: +385 1 4680-098 (M.J.), +385 1 4680-098 (P.P.). E-mail: Marijana.Juric@irb.hr (M.J.), planinic@irb.hr (P.P.).

Notes

The authors declare no competing financial interest.

■ ACKNOWLEDGMENTS

This research was supported by the Ministry of Science, Education and Sports of the Republic of Croatia (Grant Nos. 098-0982904-2946, 098-0982929-2916, and 098-1191344-2943) and by the Foundation of the Croatian Academy of Sciences and Arts. The authors are grateful to Dr. Dalibor Milić from Faculty of Science, University of Zagreb, for X-ray data collection of the single crystal.

■ REFERENCES

(1) Allen, F. H. *Acta Crystallogr.* **2002**, *B58*, 380−388.
(2) Jurić, M.; Perić, B.; Brničević, N.; Planinić, P.; Pajić, D.; Zadro, K.; Giester, G.; Kaitner, B. *Dalton Trans.* **2008**, 742−754.
(3) Jurić, M.; Perić, B.; Brničević, N.; Planinić, P.; Pajić, D.; Zadro, K.; Giester, G. *Polyhedron* **2007**, *26*, 659−672.
(4) Jurić, M.; Planinić, P.; Brničević, N.; Matković-Čalogović, D. *J. Mol. Struct.* **2008**, *888*, 266−276.
(5) Neo, K. E.; Ong, Y. Y.; Huynh, H. V.; Hor, T. S. A. *J. Mater. Chem.* **2007**, *17*, 1002−1006.
(6) Boudaren, C.; Auffrédic, J. P.; Louër, M.; Louër, D. *Chem. Mater.* **2000**, *12*, 2324−2333.
(7) Louër, M.; Louër, D.; Gotor, F. J.; Criado, J. M. *J. Solid State Chem.* **1991**, *92*, 565−572.
(8) Wada, S.; Narahara, M.; Hoshina, T.; Kakemoto, H.; Tsurumi, T. *J. Mater. Sci.* **2003**, *38*, 2655−2660.
(9) Androš, L.; Matković-Čalogović, D.; Planinić, P. *CrystEngComm* **2013**, *15*, 533−543.
(10) Nunes, G. G.; Seisenbaeva, G. A.; Kessler, V. G. *Cryst. Growth Des.* **2011**, *11*, 1238−1243.
(11) Bayot, D.; Tinant, B.; Devillers, M. *Inorg. Chem.* **2005**, *44*, 1554−1562.
(12) Thurston, J. H.; Whitmire, K. H. *Inorg. Chem.* **2003**, *42*, 2014−2023.
(13) Thurston, J. H.; Whitmire, K. H. *Inorg. Chem.* **2002**, *41*, 4194−4205.
(14) Wu, J.; Xue, D. *J. Nanoeng. Nanomanuf.* **2011**, *1*, 136−154.
(15) Wu, J.; Xue, D. *CrystEngComm* **2011**, *13*, 1966−1975.
(16) Ling, C. D.; Avdeev, M.; Kutteh, R.; Kharton, V. V.; Yaremchenko, A. A.; Fialkova, S.; Sharma, N.; Macquart, R. B.; Hoelzel, M.; Gutmann, M. *Chem. Mater.* **2009**, *21*, 3853−3864.
(17) Zhao, H.; Feng, S.; Xu, W.; Shi, Y.; Mao, Y.; Zhu, X. *J. Mater. Chem.* **2000**, *10*, 965−968.
(18) Srivastava, A. M.; Ackerman, J. F.; Beers, W. W. *J. Solid State Chem.* **1997**, *134*, 187−191.
(19) Kim, D.-W.; Kim, J.-R.; Yoon, S.-H.; Hong, K. S.; Kim, C. K. *J. Am. Ceram. Soc.* **2002**, *85*, 2759−2762.
(20) Jawahar, I. N.; Mohanan, P.; Sebastian, M. T. *Mater. Lett.* **2003**, *57*, 4043−4048.
(21) Liou, Y.-C.; Shiu, W.-H.; Shih, C.-Y. *Mater. Sci. Eng., B* **2006**, *131*, 142−146.
(22) Chen, G.-H.; Qi, B. *J. Alloys Compd.* **2006**, *425*, 395−398.
(23) Wu, S. Y.; Chen, X. M.; Yu, H. Y. *J. Eur. Ceram. Soc.* **2006**, *26*, 1973−1976.
(24) Wu, S. Y.; Chen, X. M.; Chen, L. M. *J. Electroceram.* **2008**, *21*, 810−814.
(25) Wu, S. Y.; Chen, X. M.; Liu, X. Q. *J. Alloys Compd.* **2008**, *453*, 463−469.
(26) Hsiao, Y.-J.; Chang, Y.-H.; Chang, Y.-S.; Fang, T.-H. *J. Am. Ceram. Soc.* **2007**, *90*, 2287−2290.
(27) Zhou, H.; Chen, X.; Fang, L.; Hu, C.; Wang, H. *J. Mater. Sci: Mater. Electron.* **2010**, *21*, 939−942.
(28) Bezjak, J.; Jančar, B.; Rečnik, A.; Suvorov, D. *J. Eur. Ceram. Soc.* **2008**, *28*, 2771−2776.
(29) Bezjak, J.; Rečnik, A.; Jančar, B.; Boullay, P.; Radosavljević Evans, I.; Suvorov, D. *J. Am. Ceram. Soc.* **2009**, *92*, 1806−1812.
(30) Bezjak, J.; Abakumov, A. M.; Rečnik, A.; Maček Kržmanc, M.; Jančar, B.; Suvorov, D. *J. Solid State Chem.* **2010**, *182*, 1823−1828.
(31) Leshchenko, P. P.; Lykova, L. N.; Kovba, L. M.; Stefanovich, S. Y.; Chechkin, V. V. *Inorg. Mater.* **1985**, *21*, 227−230.
(32) Leshchenko, P. P.; Paromova, M. V.; Lykova, L. N.; Kovba, L. M. *Vest. Mosk. Univ., Ser. 2: Khim.* **1979**, *20*, 148−151.
(33) Russ, F. *Z. Anorg. Chem.* **1902**, *31*, 42−91.
(34) Brničević, N.; Djordjević, C. *J. Less-Common Met.* **1976**, *45*, 45−52.
(35) Mathern, G.; Weiss, R. *Acta Crystallogr.* **1971**, *B27*, 1610−1618.
(36) *CrysAlis PRO*; Oxford Diffraction Ltd.: Abingdon, U.K., 2007.
(37) Sheldrick, G. M. *Acta Crystallogr.* **2008**, *A64*, 112−122.
(38) Spek, A. L. *J. Appl. Crystallogr.* **2003**, *36*, 7−13.
(39) Farrugia, L. J. *J. Appl. Crystallogr.* **1997**, *30*, 565.
(40) Macrae, C. F.; Edgington, P. R.; McCabe, P.; Pidcock, E.; Shields, G. P.; Taylor, R.; Towler, M.; ven de Streek, J. *J. Appl. Crystallogr.* **2006**, *39*, 453−457.
(41) Momma, K.; Izumi, F. *J. Appl. Crystallogr.* **2011**, *44*, 1272−1276.
(42) Altomare, A.; Camalli, M.; Cuocci, C.; Giacovazzo, C.; Moliterni, A.; Rizzi, R. *J. Appl. Crystallogr.* **2009**, *42*, 1197−1202.
(43) Balzar, D. *Defect and Microstructure Analysis from Diffraction*; Snyder, R. L., Bunge, H. J., Fiala, J., Eds.; IUCr/Oxford University Press: New York, 1999; pp 94−126.
(44) Šestan, M.; Perić, B.; Giester, G.; Planinić, P.; Brničević, N. *Struct. Chem.* **2005**, *16*, 409−414.
(45) Cordero, B.; Gómez, V.; Platero-Prats, A. E.; Revés, M.; Echeverría, J.; Cremades, E.; Barragán, F.; Alvarez, S. *Dalton Trans.* **2008**, 2832−2838.
(46) Nakamoto, K. *Infrared and Raman Spectra of Inorganic and Coordination Compounds*, 6th ed.; John Wiley: New York, 2009.
(47) Doi, Y.; Hinatsu, Y.; Shimojo, Y.; Ishii, Y. *J. Solid State Chem.* **2001**, *161*, 113−120.
(48) Ling, C. D.; Avdeev, M.; Kharton, V. V.; Yaremchenko, A. A.; Macquart, R. B.; Hoelzel, M. *Chem. Mater.* **2010**, *22*, 532−540.
(49) Macdonald, J. R. *Impedance Spectroscopy*; Wiley: New York, 1987.